

## Large enhancement of second harmonic generation in polymer films by microcavities

H. Cao<sup>a)</sup>

*Department of Physics and Astronomy, Northwestern University, Evanston, Illinois 60208*

D. B. Hall and J. M. Torkelson

*Department of Chemical Engineering, Northwestern University, Evanston, Illinois 60208*

C.-Q. Cao

*Department of Physics, Peking University, Beijing, 100871 People's Republic of China*

(Received 16 February 1999; accepted for publication 6 December 1999)

We report significant enhancement of second-harmonic-generation intensity in a nonlinear optical polymer by strongly confining the fundamental light in a planar microcavity. Employing a microcavity formed by a distributed Bragg reflector and a silver layer, we have observed up to a factor of 50 increase of second-harmonic light intensity in polymer thin films. © 2000 American Institute of Physics. [S0003-6951(00)04305-9]

There has been much interest and progress in the development of nonlinear optical materials for potential application in integrated optics.<sup>1,2</sup> Since the 1980's, amorphous polymers doped with nonlinear optical chromophores have been studied as promising nonlinear optical materials because of their large optical nonlinearities, low fabrication cost, and compatibility with different kinds of substrates.<sup>3-5</sup> The noncentrosymmetry needed for second-harmonic generation (SHG) is induced by the application of a dc field (poling) at temperatures near or above the glass transition temperature  $T_g$ , where the dopants can reorient and be partially aligned. However, larger optical nonlinearity is desired for many applications.

It is well known that a microcavity can modify the vacuum-field fluctuation and thus alter the decay rate and the radiation pattern of spontaneous emission.<sup>6,7</sup> Microcavities have been widely used to control luminescence characteristics of organic materials, e.g., to enhance emission intensity and directionality, narrow spectral linewidth, and tune emission frequency.<sup>8-10</sup> Nonlinear optical processes can also be modified by microcavities.<sup>11-12</sup> In this letter, we demonstrate that a planar microcavity can significantly enhance the second-order nonlinear optical response of the polymer.

The microcavity is a Fabry-Pérot cavity made of two planar mirrors. The cavity length is on the order of the optical wavelength. Figure 1 is a schematic of the sample structure. The bottom mirror is a distributed Bragg reflector (DBR), which is a stack of alternating layers of  $\text{SiO}_2$  and  $\text{TiO}_2$  on top of a BK7 glass substrate. The thickness of each layer is equal to  $\lambda_0/4n$ , where  $\lambda_0 = 1050$  nm, and  $n$  is the refractive index. The DBR stopband is centered at 1050 nm. The reflectivity of the DBR is more than 99% in the wavelength regime of 980–1110 nm. However, the DBR is transparent around 525 nm. When the fundamental wavelength is around 1050 nm, the DBR is highly reflective to the fundamental beam but transparent to the second-harmonic light. The DBR, 1 in. in diameter, is patterned with aluminum

stripes by standard photolithographic techniques. The aluminum stripes are used as planar electrodes for poling of the polymer film. The stripes are  $\sim 200$  nm thick. The distance between adjacent stripes is  $\sim 1$  mm.

Poly(methyl methacrylate) (PMMA) (4–6 wt. % polymer in solvent) and Disperse Red 1 (DR1) (4 wt % with respect to the weight of polymer) are co-dissolved in chlorobenzene, and spin coated at 2000–4000 rpm on the patterned substrates.<sup>13</sup> The films are dried first at 70 °C for 2 h and then at room temperature for 24 h. The thickness of the films is measured by a profilometer. By controlling the spin speed and the polymer concentration in chlorobenzene, the film thickness can be varied from 1 to 3  $\mu\text{m}$ . There is a slight variation in film thickness across the sample.

The films are poled by application of 1200 V across a 1 mm aluminum electrode gap ( $E \approx 1.2 \times 10^4$  V/cm). The poling temperature is 125 °C. For PMMA, the glass transition temperature  $T_g \approx 100$  °C. After poling at elevated temperature for about 15 min, the samples are cooled to 25 °C with the dc electric field still applied.

The top mirror of the cavity is a thin layer of silver. It is thermally evaporated on the PMMA film after the poling. To avoid heating of the sample, which could cause reorientation of the chromophores and loss of the nonlinear optical properties, the sample is mounted on a chilled water-cooled holder to keep it cold during thermal evaporation. In addition, a shadow mask is used to block part of the sample during the evaporation so that silver is deposited onto part of

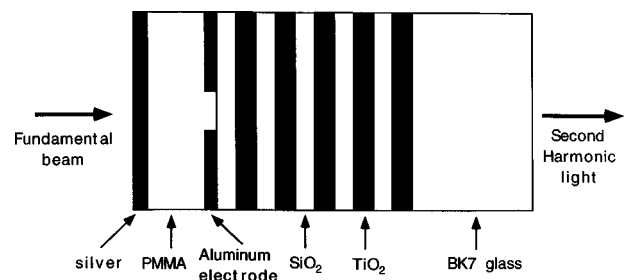


FIG. 1. Schematic of the sample structure.

<sup>a)</sup>Electronic mail: h-cao@nwu.edu

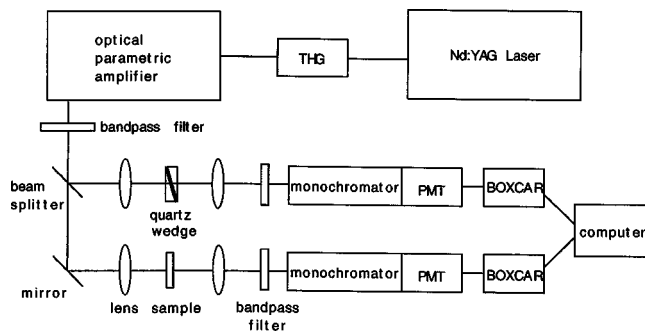


FIG. 2. Experimental setup for SHG measurement.

the PMMA film. In this way, we can compare the second-harmonic intensity from the part of the polymer film which is embedded in a microcavity to that from the part of the same film which is not in a microcavity.

SHG measurement is performed on the sample in the transmission mode. The fundamental beam, whose wavelength is around  $1.05 \mu\text{m}$ , is focused to a spot of  $400 \mu\text{m}$  in between two aluminum electrodes with normal incidence. Since the DBR is highly reflective to the fundamental light, the DBR and the silver layer form a cavity for the fundamental light. The thickness of the PMMA film is chosen so that the cavity resonant frequency is equal to the fundamental frequency. Hence, the fundamental light is accumulated inside the cavity. High intracavity fundamental light intensity leads to a very efficient second-harmonic generation in the polymer film embedded in the cavity. Since the DBR is transparent at the second-harmonic frequency, the intracavity second-harmonic light can escape from the DBR. The thickness of the silver layer is crucial to achieve efficient SHG. If the silver layer is too thick, it blocks the fundamental light from entering the cavity. If it is too thin, the cavity is too poor to effectively confine the fundamental light. In the numerical simulation, we find the transmitted second-harmonic intensity is maximal when the silver layer is 40 nm thick.

Figure 2 shows the experimental setup for the SHG measurement. The output from an active-passive mode-locked Nd:YAG laser is frequency tripled to pump an optical parametric amplifier (OPA), which operates at a 10 Hz repetition rate.<sup>14</sup> The OPA output is tunable between 0.9 and  $1.3 \mu\text{m}$ . Its spectral linewidth is  $\sim 4 \text{ nm}$ . A bandpass filter is placed near the exit port of the OPA to block the idler beam. The signal beam of the OPA is split to simultaneously generate second-harmonic light in the sample and a reference material, typically a Y-cut quartz wedge. By normalizing the second-harmonic intensity from the sample to that from the quartz wedge, the effects of pulse-to-pulse fluctuation and long-term drift in the laser power can be minimized. Two identical bandpass filters are placed after the sample and the quartz to attenuate the residual fundamental light. At each wavelength of OPA, the SHG signal from the sample and that from the quartz wedge are focused into two identical monochromators. The monochromators are tuned to the second-harmonic frequencies. Thus, only the second-harmonic signals are picked up by the monochromators. Their intensities are measured by two identical photomultiplier tubes mounted onto the exit slits of the monochromators. The second-harmonic signals are subsequently averaged

by boxcar integrators. When the monochromator is detuned from the second-harmonic frequency, the measured signal becomes zero. This test confirms that the observed signal is indeed second-harmonic light. A computer is used to control the wavelength tuning of OPA and two monochromators, as well as to acquire data from the boxcar integrators. For a better signal-to-noise ratio, the SHG signal is averaged over 200 pulses. The use of a quartz wedge as the reference material results in angular walk-off due to refraction as the fundamental wavelength is tuned, causing misalignment in the remaining detection instrumentation. To circumvent this, an X-cut quartz wedge with the same wedge angle is placed immediately after the Y-cut quartz wedge with the opposite wedge direction, thus eliminating the walk-off effect. Since the X-cut wedge generates negligible SHG, the reference signal from the Y-cut wedge is not affected. This scheme provides a uniform reference over the entire spectral tuning range without realignment. To determine the absolute value of the second-order susceptibility  $\chi^{(2)}$  of the sample, the relative SHG signal is calibrated against that generated in a Y-cut quartz plate placed at the same location as the sample and oriented at a peak in the Maker fringe pattern.<sup>14</sup> Since the quartz  $\chi^{(2)}$  has negligible dispersion in the wavelength range involved, it suffices to make the absolute calibration at one wavelength.

Figure 3(a) shows the magnitude of the effective second-order susceptibility  $\chi_{\text{eff}}^{(2)}$  measured at various fundamental wavelengths. The thickness of the DR1-doped PMMA film is  $\sim 1.13 \mu\text{m}$ . Part of the PMMA film is covered with a 40-nm-thick silver layer. The value of  $\chi_{\text{eff}}^{(2)}$  of the PMMA film without the top silver layer does not vary significantly with the fundamental frequency. In contrast, the value of  $\chi_{\text{eff}}^{(2)}$  of the same PMMA film which is embedded in the microcavity shows a sharp peak. When the fundamental frequency is equal to the cavity resonant frequency,  $\chi_{\text{eff}}^{(2)}$  is enhanced 50 times by the microcavity. However, as the fundamental frequency is tuned away from the cavity resonant frequency,  $\chi_{\text{eff}}^{(2)}$  is greatly suppressed. The linewidth of the SHG resonance peak is about 7 nm. When the fundamental beam is focused onto different positions on the film, the center wavelength of the SHG peak is shifted. This is due to the fact that the thickness of the PMMA film varies slightly across the sample, and thus the cavity resonant frequency changes with the sample position.

In order to compare with the experimental result, we have done numerical simulation of SHG enhancement by a microcavity. Using the transfer-matrix method, we calculated the distribution of the fundamental light field inside the cavity.<sup>15-17</sup> From it, we calculate the intensity of second-harmonic light generated inside the cavity and then transmitted through the DBR. The ratio of the transmitted second-harmonic light intensity from the polymer-embedded microcavity to that from a polymer film of the same thickness but without the cavity is defined as the enhancement factor. Figure 3(b) shows the calculated SHG enhancement factor versus the second-harmonic wavelength with the parameters of our sample. The polymer film is  $1.1 \mu\text{m}$  thick. The refractive index of the DR1-doped PMMA is extracted by ellipsometry. The maximal SHG enhancement factor is about 550.

The SHG enhancement observed experimentally is an

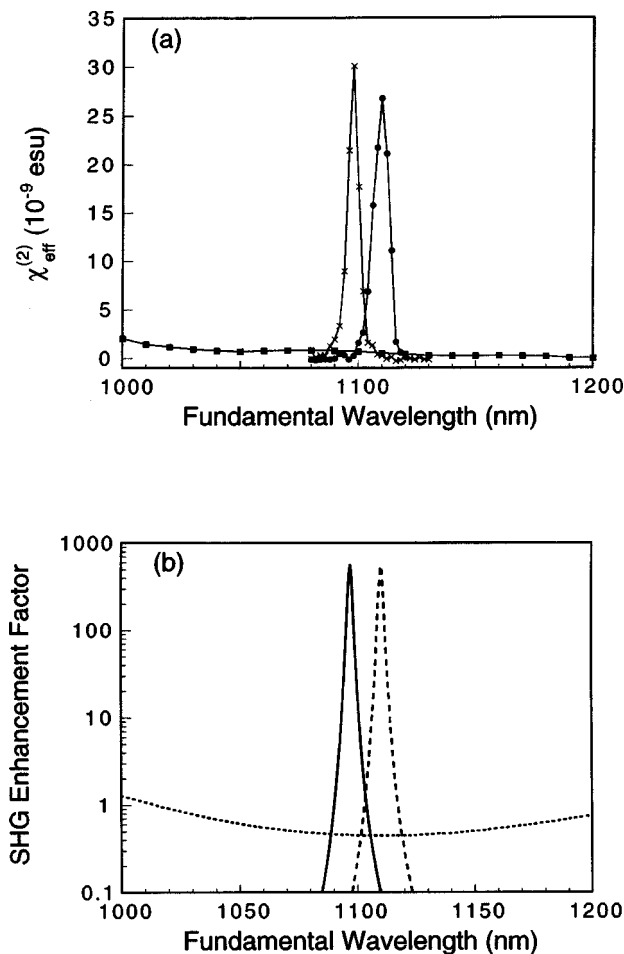


FIG. 3. (a) Circles and crosses are the measured  $\chi_{\text{eff}}^{(2)}$  of the PMMA-embedded microcavity at two different positions. The squares are the measured  $\chi_{\text{eff}}^{(2)}$  of the part of the same PMMA film without the top silver layer. The PMMA film is  $\sim 1.13 \mu\text{m}$  thick. (b) Calculated SHG enhancement factor in the PMMA-embedded microcavity. The PMMA film thickness is  $1.125 \mu\text{m}$  for the solid line, and  $1.138 \mu\text{m}$  for the dashed line. The dotted line corresponds to the PMMA film of the same thickness but without the top silver layer.

order of magnitude lower than the value predicted theoretically. This is due to the simplification made in the simulation. The fundamental light is assumed to be monochromatic in the calculation. Experimentally, the fundamental beam has a spectral linewidth  $\Delta\lambda_f \sim 4$  nm. Since the spectral bandwidth of the cavity mode  $\Delta\lambda_c \sim 1.5$  nm, only a fraction  $\Delta\lambda_c/\Delta\lambda_f \sim 0.37$  of the incident fundamental light can enter the cavity, and the rest is reflected. Thus, the SHG enhancement factor is reduced by a factor of  $(\Delta\lambda_f/\Delta\lambda_c)^2 \sim 7$ . In addition, the reabsorption of the second harmonic light is not

taken into account in the calculation. The DR1-doped PMMA has an absorption peak centered at 490 nm with a linewidth of  $\sim 100$  nm. After including the absorption of the polymer film at the second-harmonic frequency in the calculation, we find the reabsorption of the second-harmonic light by the polymer film contributes  $\sim 25\%$  reduction of the enhancement factor.

Finally, we would like to point out that the final value of  $\chi^{(2)}$  that can be achieved in the polymer-embedded microcavity depends on the value of  $\chi^{(2)}$  of the nonlinear polymer that is used. The role of a microcavity is simply magnification of the polymer's nonlinear response.

In conclusion, we have observed up to 50 times enhancement of SHG in a polymer thin film by a planar microcavity formed by a DBR and a silver layer. The cavity length is on the order of the fundamental wavelength. Strong confinement of fundamental light in a microcavity leads to significant enhancement of the SHG in the polymer film embedded in the cavity.

The authors would like to acknowledge Dr. A. DiVenero, Y. G. Zhao, J. Hooker, and M. Black for their technical assistance. This work is supported in part by the National Science Foundation under Grant No. ECS-9800068.

<sup>1</sup>M. M. Fejer, Phys. Today **47**, 25 (1994).

<sup>2</sup>A. Garito, R. F. Shi, and M. Wu, Phys. Today **47**, 51 (1994).

<sup>3</sup>K. D. Singer, J. E. Sohn, and S. J. Lalama, Appl. Phys. Lett. **49**, 248 (1986).

<sup>4</sup>D. J. Williams, in *Nonlinear Optical Properties of Organic Molecules and Crystals*, edited by D. S. Chemla and J. Zyss (Academic, Orlando, FL, 1987), Vol. 1, p. 405.

<sup>5</sup>D. M. Burland, R. D. Miller, and C. A. Walsh, Chem. Rev. **94**, 31 (1994).

<sup>6</sup>H. Yohoyama, Science **256**, 66 (1992).

<sup>7</sup>Y. Yamamoto and R. E. Slusher, Phys. Today **June** (1993).

<sup>8</sup>J. H. Burroughes, D. D. C. Bradley, A. R. Brown, R. N. Marks, K. Mackay, R. H. Friend, P. L. Burn, and A. B. Holmes, Nature (London) **347**, 539 (1990).

<sup>9</sup>A. Dodabalapur, L. J. Rothberg, R. H. Jordan, T. M. Miller, R. E. Slusher, and J. M. Phillips, J. Appl. Phys. **80**, 6954 (1996).

<sup>10</sup>D. G. Lidzey, M. A. Pate, D. M. Whittaker, D. D. C. Bradley, M. S. Weaver, T. A. Fisher, and M. S. Skolnick, Chem. Phys. Lett. **263**, 655 (1996).

<sup>11</sup>S. Nakagawa, N. Yamada, N. Mikoshiba, and D. E. Mars, Appl. Phys. Lett. **66**, 2159 (1995).

<sup>12</sup>E. Rosencher, B. Vinter, and V. Berger, J. Appl. Phys. **78**, 6042 (1995).

<sup>13</sup>A. Dhinojwala, G. K. Wong, and J. M. Torkelson, Macromolecules **25**, 7395 (1992).

<sup>14</sup>P. M. Lundquist, W. P. Lin, Z. Y. Xu, G. K. Wong, E. D. Rippert, J. A. Helfrich, and J. B. Ketterson, Appl. Phys. Lett. **65**, 1085 (1994).

<sup>15</sup>D. S. Bethune, J. Opt. Soc. Am. B **6**, 910 (1989).

<sup>16</sup>N. Hashizume, M. Ohashi, T. Kondo, and R. Ito, J. Opt. Soc. Am. B **12**, 1894 (1995).

<sup>17</sup>V. Berger, J. Opt. Soc. Am. B **14**, 1351 (1997).